
MC²: Monte Carlo Correction for Fast Elliptic PDE Solving

Ethan Hsu*

Stanford University
ethanhhsu@stanford.edu

Ivan Ge*

Stanford University
ivange@stanford.edu

Hong Meng Yam*

Stanford University
hongmeng@stanford.edu

Abstract

Partial differential equation (PDE) solvers underpin scientific computing, but real-world deployment is bounded by compute. Classical Monte Carlo solvers such as Walk-on-Spheres (WoS) are unbiased and geometry-agnostic but are slow. Learned solvers are fast but biased and brittle under distribution shift. We present **MC²**, a hybrid WoS-Neural Network (WoS-NN) PDE solver that treats a low-budget Monte Carlo solution as a structured estimator of the true field and learns a single-pass neural correction to recover a high-fidelity solution. **MC²** matches the accuracy of solutions using over $1000\times$ more Monte Carlo compute, outperforming all evaluated classical, denoising, and neural-operator baselines. To enable reproducible study of finite-compute PDE solving, we additionally release **PDEZoo**, the largest standardized elliptic PDE benchmark to date: 2M PDEs spanning five elliptic families and unlimited geometric compositions, with analytic ground truth and multi-budget Monte Carlo trajectories. Together **MC²** and **PDEZoo** (1) empirically establish that finite-sample Monte Carlo error is structured, learnable, and correctable in a single forward pass, (2) show that we can solve PDEs $\sim 1000\times$ faster than with just WoS, and (3) provide the evaluation infrastructure the field has so far lacked.

1 Introduction

Elliptic partial differential equations (PDEs) are a core computational primitive across scientific computing, geometry processing, and computer graphics, critical for tasks such as reconstruction, simulation, and physical modeling [3, 6, 15]. In practice, solvers must operate reliably across diverse forcing functions, boundary conditions, and geometries, while remaining fast enough for large-scale or latency-sensitive pipelines. Despite decades of progress, we lack approaches that simultaneously achieve generality, accuracy, and efficiency in this regime.

Classical deterministic solvers such as finite difference and finite element methods (FDM/FEM) can be highly accurate, but rely on explicit meshing and problem-specific discretization choices that limits flexibility on irregular domains [5, 4, 30]. Monte Carlo solvers, most notably Walk-on-Spheres (WoS), address many of these limitations. They are mesh-free, unbiased, and applicable to broad classes of elliptic PDEs and geometries [27, 30, 31]. However, their finite-iteration outputs suffer from high variance, requiring orders of magnitude more samples to reach acceptable accuracy [32].

Learning-based solvers, such as PINNs, neural operators, transformer models, offer fast inference but introduce bias, and can fail under distribution shifts or unseen PDE specifications [1, 21, 7, 23]. Recent hybrid approaches integrate neural networks into Monte Carlo solvers (e.g., neural caches [38]) or condition generative models on sparse numerical samples [16], but require per-problem retraining, slow iterative inference, or both.

In this work, we propose **MC²** (Monte Carlo error correction with Monte Carlo solvers): a new approach to hybrid PDE solving that treats the low-iteration output of a Monte Carlo method as

a structured estimator of the true solution and learns a neural network correction that reduces error in a single forward pass. Rather than modifying a Monte Carlo solver or replacing it with a learned surrogate, MC² applies a transformer-based field-to-field model to early Walk-on-Spheres outputs, recovering solution quality that would otherwise require around 1000× more Monte Carlo iterations [10]. This preserves the generality and robustness of Monte Carlo solvers while dramatically accelerating convergence and lowering the bias of standalone neural solvers.

To support this setting and enable reproducible evaluation, we introduce PDEZoo, a benchmark offering nearly limitless diversity within the elliptic PDE regime. PDEZoo spans Laplace, Poisson, Yukawa, Biharmonic, and Helmholtz equations with explicit forcing functions, boundary conditions, and dense reference solutions. Unlike existing PDE benchmarks, PDEZoo is designed for finite-compute evaluation: it includes Monte Carlo solver trajectories at multiple compute budgets, exposing how solvers behave before asymptotic convergence and allowing methods to be compared under practical resource constraints. We further release the full procedural generator, enabling arbitrarily large training sets while preserving a fixed benchmark for standardized evaluation.

Our contributions are twofold:

1. **MC²**, a hybrid WoS–NN solver that corrects structured Monte Carlo error across diverse elliptic PDEs, matching the quality of using 512–2,048× more Monte Carlo compute and outperforming all evaluated baselines. In other words, it combines the generality and unbiasedness of Monte Carlo PDE solvers with learned error correction to yield a more than 1000x wall-clock speedup on PDE solving without sacrificing robustness.
2. **PDEZoo**, the largest standardized benchmark to date for elliptic PDEs with explicit forcing and boundary functions, augmented with Monte Carlo solver trajectories and a scalable procedural generator.

2 Related Work

Monte Carlo PDE Solvers: Walk-on-Spheres (WoS) estimates solutions to elliptic PDEs via random walks guided by Green’s functions [27]. Since WoS is mesh-free and unbiased, it extends to irregular geometries and has been generalized to mixed Dirichlet–Neumann conditions [32], boundary integral formulations [33], and Monte Carlo finite element settings [19]. These properties make WoS attractive for graphics and simulation [30, 31]. However, the estimator variance decays only as $\mathcal{O}(1/K)$, meaning that the typical estimation error decays only as $\mathcal{O}(1/\sqrt{K})$. As a result, reaching acceptable accuracy in budget-constrained settings can require prohibitively many samples.

Neural Networks for PDEs: Physics-informed neural networks (PINNs) enforce PDE residuals through specialized loss functions [1, 18, 28], while neural operators such as FNO learn mappings between function spaces [24]. More recent work has explored generative approaches using diffusion models. DiffusionPDE conditions a diffusion model on sparse observations to jointly recover coefficients and solutions while CoCoGen augments score-based sampling with PDE-residual guidance to improve physical consistency [16, 17]. Transformer-based architectures have further enabled fast inference and some degree of cross-PDE generalization. However, neural solvers face non-convex loss landscapes, spectral bias [37, 29], and distribution-shift fragility, producing biased solutions that degrade on out-of-distribution problems [23, 7].

Hybrid Monte Carlo-Neural Network Methods: Recent work combines neural networks with Monte Carlo solvers to retain unbiasedness while reducing variance. Li et al. [23] train a neural field to approximate the PDE solution, then use it as a control-variate cache during WoS sampling. While effective, this requires per-problem training and manual hyperparameter tuning. Diffusion-based approaches condition generative models on sparse numerical samples to reconstruct full solution fields [16], but suffer from slow multi-step inference and conditioning instability [20]. Our approach differs in two key ways: (i) the corrector is trained once across the entire PDE distribution rather than per-instance, and (ii) correction is a single deterministic forward pass, not iterative sampling.

Benchmarks and Scientific Progress. Despite a rapidly growing literature on neural and hybrid PDE solvers, the field lacks the unified, standardized evaluation infrastructure that has driven progress in adjacent areas of machine learning. Donoho [9] argues that “frictionless reproducibility”, fostered by shared tasks, common data, and open leaderboards, was the engine behind transformative progress

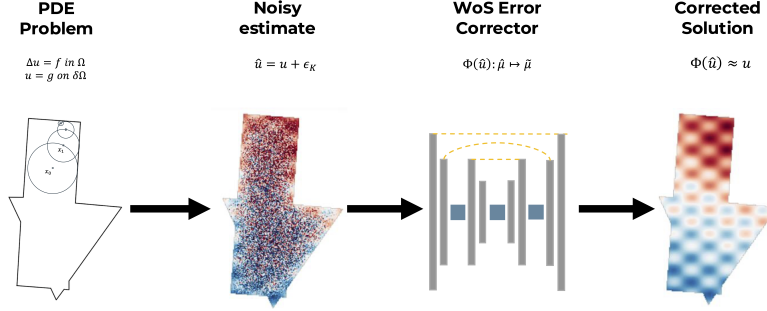


Figure 1: **MC² pipeline.** A low-budget Monte Carlo WoS estimate is corrected in a single forward pass by a learned operator, yielding an improved solution for the PDE.

in NLP and computer vision, where benchmarks like GLUE [35], SuperGLUE [36], and ImageNet [8] created a culture of head-to-head comparison on identical inputs. PDE solving has no analog. Existing benchmarks each occupy narrow regimes: PDEBench [34] and PDEArena [12] target time-dependent PDEs on fixed rectangular grids; the FNO datasets [?] ship a small number of canonical problems on the unit square; and Poseidon [14], while large-scale, is restricted to fixed grids and uses numerical solver outputs as ground truth. Crucially, none of these benchmarks support *finite-compute* evaluation: they provide a single converged solution per instance, with no visibility into solver behavior at intermediate sample budgets. They also lack analytic ground truth, conflating model error with discretization error from the reference solver. Furthermore, they all lack a maintained leaderboard and sufficient test sizes for the community to accurately track State-Of-The-Art results. As a result, comparisons across papers in this space are typically apples-to-oranges, and there is no shared standard against which new methods are evaluated. We designed PDEZoo to fill this gap.

3 Methodology: Monte Carlo Error Correction

We introduce a framework for accurate yet extremely fast elliptic PDE solving in the finite-compute regime, where classical Monte Carlo solvers are unbiased but often dominated by variance [27]. We begin by formalizing Monte Carlo PDE solvers as unbiased but stochastic estimators, then introduce a learned estimator correction framework and its neural instantiation. Importantly, our approach substantially reduces estimator variance while introducing only bounded bias, yielding a favorable bias–variance tradeoff that we analyze in Appendix F.

Problem Setting and PDE Families

We consider elliptic partial differential equations of the following form with Dirichlet boundary conditions:

$$\begin{cases} \nabla \cdot (\alpha(x)\nabla u(x)) + \omega(x)\nabla u(x) - \sigma(x)u(x) = -f(x), & x \in \Omega \\ u(x) = g(x), & x \in \partial\Omega \end{cases} \quad (1)$$

where α, ω, σ are spatially varying coefficients, f is the forcing function, g is the boundary function, and Ω is specified via a signed distance function [23].

Monte Carlo PDE Solvers as Unbiased Stochastic Estimators

Monte Carlo solvers such as Walk-on-Spheres (WoS) express the solution $u(x)$ as the expectation of a random process derived from Green’s functions: $u(x) = S(x) + \mathbb{E}[u(Y)]$, where Y denotes the next random walk location and $S(x)$ aggregates source terms. In practice, this expectation is approximated with K samples: $\hat{u}_K(x) = \frac{1}{K} \sum_{k=1}^K u(Y_k)$, which satisfies $\mathbb{E}[\hat{u}_K(x)] = u(x)$ and $\text{Var}[\hat{u}_K(x)] = \mathcal{O}(1/K)$. Although unbiased, \hat{u}_K is dominated by variance at small K , severely limiting accuracy in budget-constrained regimes.

Finite-Compute Estimator Correction

Rather than modifying the Monte Carlo solver, we adopt an estimator-centric perspective and treat the finite-budget output as a noisy observation $\hat{u}_K = u + \varepsilon_K$, where ε_K is zero-mean, heteroskedastic, and spatially correlated noise induced by finite sampling. Thus, we seek a corrected estimator

Table 1: Comparison of PDE benchmarks. PDEZoo is the only benchmark combining exact analytic ground truth, diverse per-instance geometries, multi-budget stochastic solver data, and a scalable procedural generator.

Benchmark	PDE Scope	Geometries	Analytic Ground Truth	Intermediate Solutions	Procedural Generator	Scale
PDEBench [34]	Time-dep. PDEs	Fixed grids	✗	✗	✗	~10k
PDEArena [12]	Time-dep. PDEs	Fixed grids	✗	✗	✗	~5–10k
FNO datasets [24]	Canonical PDEs	Unit square	✗	✗	✗	~ 7k
Poseidon [14]	Multi-PDE	Fixed grids	✗	✗	✗	1.6M
PDEZoo	Elliptic (5 families)	Unlimited (8 primitives)	✓	✓	✓	2M

$\tilde{u} = \Phi(\hat{u}_K)$ that minimizes mean-squared error under fixed compute. Under squared loss, the optimal mapping is $\Phi^*(\hat{u}_K) = \mathbb{E}[u \mid \hat{u}_K]$, which trades unbiasedness for variance reduction. Since Φ^* is intractable, we learn an approximation Φ_θ via:

$$\min_{\theta} \mathbb{E} [\|\Phi_\theta(\hat{u}_K) - u\|_2^2], \quad (2)$$

using ground truth solutions as supervision. Crucially, Φ_θ operates purely as a post-processing correction: it does not need PDE coefficients, boundary conditions, or solver internals at inference time.

Field Discretization

For learning and evaluation, continuous solution fields are discretized on uniform grids, yielding arrays $U \in \mathbb{R}^{H \times W}$. This discretization is used solely for numerical representation. Each training pair consists of a low-budget Monte Carlo estimator \hat{U}_K and a reference solution U^* . The learning problem is therefore a field-to-field regression from stochastic estimators to ground truth. We note that our method can be extended to arbitrary discretizations without retraining by evaluating the Monte Carlo estimator on a finer discretization and applying the learned correction in a sliding-window fashion.

Neural Estimator Correction

We parameterize Φ_θ by using a modified SUNet (Swin-UNet), a transformer-based encoder–decoder originally developed for image restoration. Its multi-scale hierarchy, shifted-window attention, and skip connections make it well-suited for modeling the long-range, spatially structured error induced by Monte Carlo sampling. At **inference time**, we run a Monte Carlo solver at budget K to obtain \hat{u}_K and apply the learned correction $\tilde{u} = \Phi_\theta(\hat{u}_K)$ in a single forward pass. The correction step incurs constant-time overhead.

4 PDEZoo: A Large-Scale Benchmark for Elliptic PDEs

We introduce **PDEZoo**, a large-scale benchmark for elliptic partial differential equations (PDEs). It is intended to evaluate numerical, learning-based, and hybrid solvers in the *finite-compute* regime. Each instance provides (i) an explicit elliptic boundary-value problem with Dirichlet boundary conditions, (ii) a known *analytic* solution used as ground truth, and (iii) optional multi-budget trajectories produced by a Monte Carlo solver.

PDEZoo is the only benchmark combining exact analytic ground truth, diverse per-instance geometries, multi-budget stochastic solver data, and a scalable procedural generator (Table 1), allowing us to benchmark solver performance at various compute levels within a unified and reproducible evaluation protocol.

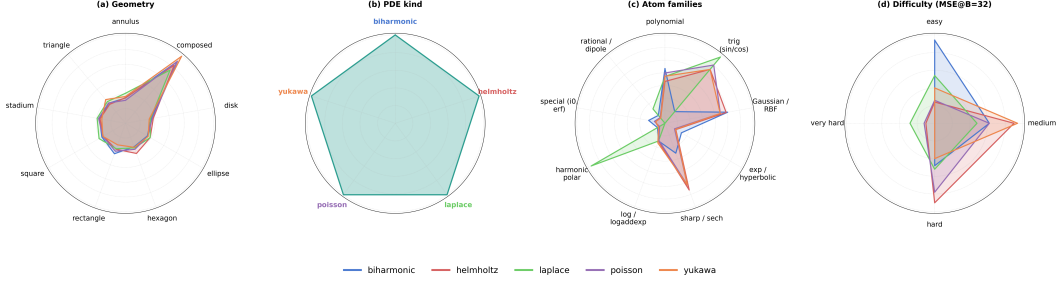


Figure 2: Overview of Data Distribution PDEZoo

4.1 Problem Specification

Each PDE instance is defined by a tuple $\mathcal{P} = (\Omega, \mathcal{E}, f, g, u)$, where $\Omega \subset \mathbb{R}^d$ is a bounded domain with boundary $\partial\Omega$, \mathcal{E} denotes an elliptic PDE family, $f : \Omega \rightarrow \mathbb{R}$ is a forcing term, $g : \partial\Omega \rightarrow \mathbb{R}$ specifies Dirichlet boundary conditions, and $u : \Omega \rightarrow \mathbb{R}$ is the analytical solution. PDEZoo includes five elliptic PDE families:

$$\begin{aligned} \text{Laplace: } \Delta u &= 0, & \text{Poisson: } \Delta u &= f, & \text{Yukawa: } \Delta u - \lambda u &= f, \\ \text{Biharmonic: } \Delta^2 u &= f, & \text{Helmholtz: } \Delta u + k^2 u &= f. \end{aligned}$$

all posed in Ω with Dirichlet boundary condition $u = g$ on $\partial\Omega$. For each family, u is analytically specified and the corresponding right-hand side f and boundary values g are derived exactly from u . Additional details on the manufactured solution families and parameter ranges are provided in Appendix A.7.

4.2 PDEZoo Generation

Each instance is generated by the following procedure. First, we sample a PDE family (Laplace, Poisson, or Yukawa, each with probability $1/3$) and a domain Ω , with the latter drawn uniformly from one of eight primitive shapes or a Boolean composition of two primitives. We then construct an analytic solution u via the *method of manufactured solutions*: u is defined as a random sum of n atom functions drawn from a curated pool, and the forcing term f and boundary condition g are derived analytically from u and the selected PDE family. This yields a fully specified boundary value problem with a known analytic solution.

Solution atoms. The atom pool is designed to span the spectrum of features that arise in real elliptic PDE solutions: smooth low-frequency modes (polynomials, plane waves), localized structures (Gaussian bumps, radial basis functions), singularity-like behavior (log sources, rational functions), and sharp gradients (tanh transitions, high-frequency products). Using these atoms, PDEZoo contains 2 million elliptic PDE instances across Laplace, Poisson, Yukawa, Helmholtz, and Biharmonic families.

Domains. Domains are represented implicitly through signed distance functions (SDFs), which support geometry evaluation, boundary projection, and interior/boundary sampling. PDEZoo includes eight primitive domain families (disk, square, rectangle, ellipse, annulus, triangle, hexagon, and stadium) as well as composed domains formed by Boolean operations (union, intersection, difference) on two or more primitives. Composed SDFs are conservative underestimates of the true boundary distance, preserving WoS correctness (Appendix A.2).

Ground truth. Ground-truth labels are given by evaluating the analytic solution u on a fixed 256×256 grid over pixel space.

4.3 Finite Compute Monte Carlo Partial Solutions

For each PDE instance, PDEZoo includes intermediate Monte Carlo WoS solver outputs at a set of budgets $\mathcal{B} = \{B_1 < \dots < B_m\}$, producing a trajectory $\{\hat{u}_B\}_{B \in \mathcal{B}}$ evaluated on the same grid as u . These trajectories expose finite-sample estimator behavior and allow models to be trained or

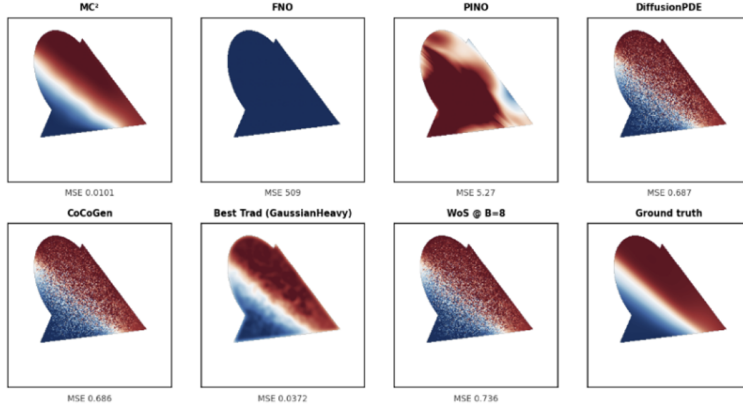


Figure 3: **Qualitative comparison of MC^2 against baselines on a Poisson instance.** MC^2 closely matches analytic ground truth and neural operators perform poorly. DiffusionPDE, CoCoGen, and raw WoS at $B=8$ all retain substantial noise, and the best traditional denoiser over-smooths boundaries.

evaluated using intermediate solutions. Budget sets, storage format, and reproducible generation details are in Appendix A.4.

4.4 Splits, Tasks, and Evaluation Protocol

Fixed benchmark splits. PDEZoo releases fixed splits for full reproducibility and to prevent training on test set data. The train split contains 2,000,000 Laplace, Poisson, and Yukawa instances with WoS solutions at budgets $\mathcal{B}_{\text{train}} = 1, 2, 4, 8, 16, 32$. The out-of-distribution test split contains 5,000 instances across Laplace, Poisson, Yukawa, Helmholtz, and Biharmonic, with WoS solutions at 20 budgets from $B = 1$ to $B = 131,072$. Helmholtz and Biharmonic instances are reserved for testing to evaluate generalization across PDE types. Each instance stores three 256×256 float32 arrays per budget: the WoS estimate, analytic ground truth, and domain mask.

Evaluation Settings. PDEZoo supports three evaluation settings on each PDE type:

- (a) Dense-field solving: predict u on the evaluation grid given $(\Omega, \mathcal{E}, f, g)$
- (b) Finite-compute correction: given a low-budget estimate \hat{u}_B , produce an improved estimate under fixed compute.
- (c) Point-query evaluation: estimate $u(x)$ at queried points $x \in \Omega$.

Difficulty calibration. A useful benchmark requires a controlled spread of instance difficulty. We classify instances into four tiers based on MSE at the reference budget $B = 32$ (Table 8). See Appendix A.6 for more details.

5 Experiments

5.1 Training Regime

We train all methods on the same random subset of 100,000 elliptic PDE from PDEZoo’s training split. Each instance consists of a PDE specification (forcing function f , boundary condition g , and domain Ω), a Monte Carlo Walk-on-Spheres (WoS) solution at budget of $B = 8$, and the corresponding analytic ground truth solution u . We use a subset of 5,000 PDEs from the PDEZoo training split for training validation, and use it for early stopping and hyperparameter selection.

For MC^2 , we train using data from MC budgets of $B \in \{2^n\}_{n=2}^5$ and their respective source terms, with an error-correction objective using our analytical ground truth as the target output. During inference, the $B = 8$ WoS solutions (noisy estimates) and the source term are inputted into the model.

For baselines trained to learn operators, the inputs are the forcing functions f evaluated on the same grid. For diffusion baselines, we train a separate EDM teacher per PDE family on the joint distribution

Table 2: MC² matches the accuracy of orders-of-magnitude more Monte Carlo compute and outperforms all other neural network methods on PDEZoo. Evaluation are on the 5,000-instance PDEZoo test set, with metrics averaged across all five elliptic PDE families (Biharmonic, Helmholtz, Laplace, Poisson, and Yukawa). Arrows indicate best metric direction. Bold marks the best result per column among learned and post-processing methods.

METHOD	PSNR (dB) \uparrow	SNR (dB) \uparrow	MSE \downarrow	LPIPS \downarrow
<i>Walk-on-Spheres (Monte Carlo)</i>				
WoS ($B=8$)	15.26 \pm 7.43	9.773 \pm 7.527	(8.02 \pm 8.34) $\times 10^{-2}$	0.7275 \pm 0.4198
WoS ($B=16384$)	42.14 \pm 13.82	36.644 \pm 13.843	(3.13 \pm 12.43) $\times 10^{-3}$	0.1964 \pm 0.3088
WoS ($B=32768$)	44.98 \pm 13.92	39.486 \pm 13.935	(1.88 \pm 8.77) $\times 10^{-3}$	0.1592 \pm 0.2731
WoS ($B=65536$)	47.80 \pm 14.00	42.307 \pm 14.009	(1.11 \pm 6.15) $\times 10^{-3}$	0.1263 \pm 0.2381
<i>Traditional Denoisers (applied to $B=8$ WoS)</i>				
GAUSSIAN	18.85 \pm 8.31	13.361 \pm 8.253	(5.06 \pm 6.96) $\times 10^{-2}$	0.4032 \pm 0.2520
GAUSSIAN (HEAVY)	17.66 \pm 6.48	12.164 \pm 6.307	(4.06 \pm 5.04) $\times 10^{-2}$	0.2832 \pm 0.2062
TOTAL VARIATION	24.63 \pm 10.41	19.141 \pm 10.419	(2.71 \pm 4.86) $\times 10^{-2}$	0.2613 \pm 0.2123
NON-LOCAL MEANS	26.63 \pm 10.36	21.134 \pm 10.444	(1.93 \pm 3.94) $\times 10^{-2}$	0.3212 \pm 0.3014
<i>Neural Network Methods</i>				
FNO	7.74 \pm 5.47	2.251 \pm 4.846	(2.58 \pm 1.57) $\times 10^{-1}$	0.3790 \pm 0.2277
PINO	8.24 \pm 6.13	2.745 \pm 5.878	(2.49 \pm 1.57) $\times 10^{-1}$	0.3753 \pm 0.2236
CoCoGen	8.25 \pm 2.92	2.674 \pm 3.631	(1.78 \pm 0.91) $\times 10^{-1}$	0.5597 \pm 0.2522
DIFFUSIONPDE	8.25 \pm 2.92	2.674 \pm 3.632	(1.78 \pm 0.91) $\times 10^{-1}$	0.5600 \pm 0.2525
MC² (OURS)	44.90 \pm 12.49	39.410 \pm 12.532	(1.94 \pm 11.38) $\times 10^{-3}$	0.0164 \pm 0.0681

($u, f, \lambda, mask$) with the standard score-matching loss and DiffusionPDE or CoCoGen as the sampler so no MC observation enters training.

5.2 Comparisons

Walk-on-Spheres (WoS). We evaluate raw WoS solutions across a range of sampling budgets: $B \in \{8, 16, 32, 64, 256, 1,024, 4,096, 16,384\}$ walks per grid point. These provide unbiased but variance-dominated estimates of the true solution, with accuracy improving on the order of $\mathcal{O}(1/\sqrt{B})$.

Traditional Denoisers. We apply six classical denoising algorithms to budget $B = 8$ WoS outputs: gaussian filtering, median filtering, bilateral filtering, total variation minimization, and non-local means. These methods assume generic noise models and do not leverage PDE-specific structure.

Neural Operator Models. We evaluate FNO [24] and PINO [25] in the operator learning setting, where the input is the forcing function f and the target is the solution u . PINO uses the same FNO architecture with an additional physics loss term,

$$\mathcal{L} = \mathcal{L}_{\text{data}} + \lambda \mathcal{L}_{\text{physics}}, \quad \lambda = 0.1,$$

where $\mathcal{L}_{\text{data}}$ is the MSE to ground truth and $\mathcal{L}_{\text{physics}}$ penalizes Laplacian inconsistency.

Diffusion Models. We evaluate DiffusionPDE and CoCoGen, two SOTA PDE solvers built on a per-PDE-family EDM. Since these models must be trained on a particular PDE family and are not generalizable, we report results only for PDE families in our train set for these models: Laplace, Poisson, and Yukawa.

5.3 Evaluation Results

We evaluate on the 5,000-instance PDEZoo test split and present our quantitative results across all methods in Table 2. Our MC² corrector achieves 44.10dB PSNR from budget $B = 8$ input, which is an improvement of 31.6 dB over the raw $B = 8$ WoS estimate (25.54 dB) and surpassing WoS at $B = 16,384$ (2048 \times more compute). MC² outperforms all other methods such as FNO [24], PINO [25], and CoCoGen [17] across all metrics. We also show strong scaling at every metric

Generalization to Out-of-Distribution (OOD) PDE Families: Additionally, we show that MC² generalizes well to OOD PDE families, as seen in Table 3, which is a huge advantage over previous SOTA diffusion-based methods who are unable to generalize outside single PDE families.

Table 3: Per-family PSNR (dB, \uparrow) on the PDEZoo test set. MC² achieves the highest PSNR on every PDE family compared to other Neural Network methods, including the held-out Biharmonic and Helmholtz families absent from the training distribution. CoCoGen and DiffusionPDE are trained per-family on in-distribution PDEs only and cannot be evaluated on held-out families. MC² uses a single $B=8$ WoS input. Bold marks the best result per column among learned and post-processing methods. Full per-family breakdown on SNR, MSE and LPIPS can be found in Appendix E.1.

METHOD	In-distribution				Out-of-distribution		
	LAPLACE	POISSON	YUKAWA	AVERAGE	BIHARMONIC	HELMHOLTZ	AVERAGE
<i>Walk-on-Spheres (Monte Carlo)</i>							
WoS ($B=8$)	25.22 \pm 3.33	11.20 \pm 5.25	13.89 \pm 5.88	16.82 \pm 7.84	15.01 \pm 6.38	10.93 \pm 5.01	12.96 \pm 6.09
WoS ($B=8192$)	55.29 \pm 3.42	32.94 \pm 11.73	38.83 \pm 10.08	42.41 \pm 13.18	37.30 \pm 13.76	32.05 \pm 11.88	34.67 \pm 13.12
WoS ($B=16384$)	58.30 \pm 3.42	35.86 \pm 11.85	41.81 \pm 10.11	45.38 \pm 13.25	39.77 \pm 13.91	34.89 \pm 12.08	37.32 \pm 13.25
WoS ($B=32768$)	61.31 \pm 3.42	38.81 \pm 11.92	44.80 \pm 10.12	48.37 \pm 13.29	42.15 \pm 13.98	37.77 \pm 12.22	39.95 \pm 13.31
<i>Traditional Denoisers (applied to $B=8$ WoS)</i>							
GAUSSIAN	29.67 \pm 2.56	14.64 \pm 6.57	17.57 \pm 6.09	20.68 \pm 8.46	18.11 \pm 7.59	14.21 \pm 6.40	16.15 \pm 7.29
GAUSSIAN (HEAVY)	25.98 \pm 3.30	14.64 \pm 4.95	16.55 \pm 4.87	19.10 \pm 6.67	16.73 \pm 5.82	14.32 \pm 4.98	15.52 \pm 5.55
TOTAL VARIATION	37.81 \pm 2.63	19.34 \pm 8.60	23.34 \pm 7.77	26.89 \pm 10.51	23.81 \pm 9.62	18.80 \pm 8.29	21.29 \pm 9.32
NON-LOCAL MEANS	39.16 \pm 3.05	21.56 \pm 8.85	25.54 \pm 7.71	28.81 \pm 10.31	25.91 \pm 9.90	20.88 \pm 8.48	23.39 \pm 9.56
<i>Neural Network Methods</i>							
FNO	16.52 \pm 5.94	5.47 \pm 1.84	5.68 \pm 1.93	9.27 \pm 6.41	5.43 \pm 2.36	5.52 \pm 1.99	5.47 \pm 2.18
PINO	18.46 \pm 6.15	5.71 \pm 1.95	5.65 \pm 1.89	10.00 \pm 7.20	5.54 \pm 2.32	5.70 \pm 2.19	5.62 \pm 2.26
CoCoGen	7.15 \pm 3.68	8.78 \pm 2.21	8.85 \pm 2.30	8.25 \pm 2.92	—	—	—
DIFFUSIONPDE	7.15 \pm 3.68	8.78 \pm 2.21	8.84 \pm 2.30	8.25 \pm 2.93	—	—	—
MC² (OURS)	59.94 \pm 3.85	42.17 \pm 9.54	46.40 \pm 8.21	49.55 \pm 10.75	35.96 \pm 13.25	40.05 \pm 9.42	38.01 \pm 11.67

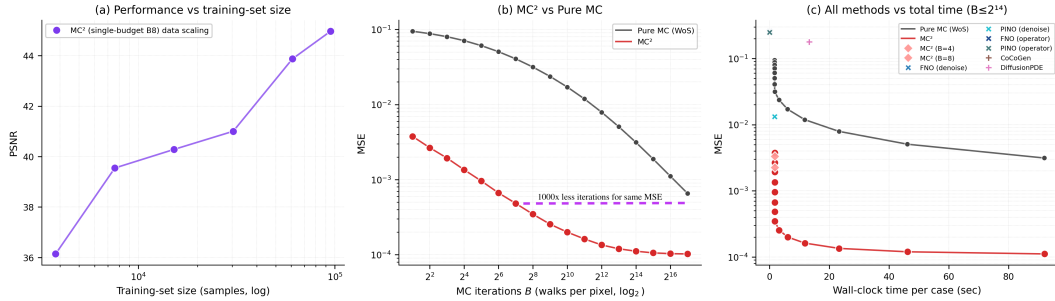


Figure 4: **Scaling Study of MC²** (a) MC² performance scales smoothly with training-set size at fixed input budget $B=8$, with no sign of saturation. (b) We evaluate performance of applying MC² error corrector to different WoS budgets. At every WoS budget, MC² achieves substantially lower MSE than input WoS budget, matching the accuracy of $\sim 1,000\times$ more MC compute. (c) On the accuracy–compute Pareto frontier, MC² dominates all evaluated baselines across the entire wall-clock range.

5.4 MC² Ablations

Multi-budget vs. single-budget training. Our MC² model is trained jointly on noisy Walk-on-Spheres solutions at budgets $B \in \{1, 2, 4, 8, 16, 32\}$. We compare this model against single-budget baselines, which are trained using only one input budget. When evaluating on our test set where the input is a single noisy Walk-on-Spheres solution at $B=8$, the multi-budget model improves performance by roughly 0.7–0.8 dB.

Source-term conditioning. To quantify the importance of conditioning on the PDE source term f , we compare models trained without f against the full MC² model at the same budget. In particular, removing f in reduces performance by approximately 6.8 dB at $B=4$.

Loss precision. We compare two models trained at $B=8$, one of which accumulates the loss in FP32, and the other which uses BF16. The FP32-loss model reaches 57.7 dB PSNR, compared to 54.8 dB for the BF16-loss model.

Data scaling. We train five MC² models using 4%, 8%, 16%, 32%, and 64% of the training set. All runs use the same hyperparameters, so differences in performance primarily reflect the amount of available training data. These runs trace a data-scaling curve for MC² at a fixed Monte Carlo input budget.

6 Discussion

Finite-sample Monte Carlo error is structured, learnable, and correctable. The central empirical claim of this work is that the residual $\varepsilon_K = \hat{u}_K - u$ produced by a low-budget WoS solver is not well-modeled as spatially independent noise, but carries structure that is consistent across PDE instances and recoverable by a learned operator. Three observations support this, each ruling out a distinct alternative hypothesis:

- **Against an unstructured-noise model.** Generic denoisers that assume locally-stationary noise (Gaussian, total variation, non-local means) plateau below 27 dB on $B = 8$ inputs, while MC^2 reaches 44.10 dB on the same inputs (Table 2). Since the baselines are non-parametric, the 17 dB gap is a measured lower bound on the information content of ε_K that pointwise noise models cannot exploit.
- **Against a pure solution-prior explanation.** FNO trained on the same data with direct access to (f, g, Ω) achieves 30.34 dB, which is 13.76 dB below MC^2 despite having strictly more direct information about the target. The corrector therefore exploits joint statistics of (\hat{u}_K, u) that are not recoverable from the PDE specification alone.
- **Against a family-specific structure.** MC^2 generalizes zero-shot to held-out Biharmonic and Helmholtz families (34.88 and 35.87 dB), within 4–5 dB of its in-distribution Poisson performance. Because these operators are qualitatively different (fourth-order and indefinite), the transfer is consistent with the corrector having learned features of the WoS estimator’s finite-sample behavior, such as boundary-induced correlations, geometry-dependent variance scaling, rather than family-specific solution priors.

We emphasize the scope of this claim. Our evidence establishes that finite-sample WoS error on 2D elliptic problems contains learnable structure sufficient to recover ~ 30 dB from a single $B = 8$ estimate; we do not claim the structure admits a closed-form description, that the learned corrector is Bayes-optimal, or that comparable gains transfer to arbitrary stochastic solvers. The bias–variance analysis in Appendix F formalizes when a Lipschitz corrector strictly reduces MSE relative to the underlying unbiased estimator, but the empirical magnitude is a property of the WoS–elliptic-PDE pair we study.

Beyond Walk-on-Spheres: A General Recipe for Unbiased Estimators. Although we instantiate Monte Carlo error correction with WoS, nothing in the framework is specific to PDEs or to walk-based estimators. The key requirements are simply (i) an unbiased stochastic estimator \hat{u}_K whose finite-budget error has learnable structure, such as spatially or temporally correlated bias-free noise induced by geometry, sampling distribution, or problem parameters, and (ii) access to high-fidelity reference outputs or ground truths for supervision. These conditions are met by a wide range of estimators across scientific computing and machine learning: path-traced rendering, Markov chain Monte Carlo posterior sampling, particle filters, neutron transport simulations, and quantum Monte Carlo. In each case, finite-sample error exhibits the same kind of structured, distribution-specific patterns that a learned corrector can exploit. We view MC^2 as the first instance of a broader paradigm: *train once across the problem distribution*, then convert any unbiased sampler into a fast, single-pass estimator while retaining bounded unbiasedness from the underlying unbiased solver. Extending the framework to these other domains is an immediate direction for future work.

7 Conclusion

We make two contributions to elliptic PDE solving in the finite-compute regime. MC^2 establishes that finite-sample Monte Carlo error is structured and correctable in a single forward pass, achieving the accuracy of over 1000x more sampling compute and outperforming all evaluated baselines, including on out-of-distribution PDE families. **PDEZoo** provides the infrastructure the field has so far lacked: 2M elliptic PDEs with analytic ground truth and multi-budget Monte Carlo trajectories. A main limitation is that we can only solve the class of PDEs that Walk-on-Spheres can solve, which are broadly elliptic problems on domains where the Green’s-function machinery applies, and extending the framework to hyperbolic, parabolic, or strongly nonlinear regimes will require pairing it with a different unbiased estimator. Within that scope, however, MC^2 closes most of the gap to high-budget Monte Carlo at a fraction of the cost, and we see the same recipe as a template for the broader family of unbiased Monte Carlo solvers.

References

- [1] Jens Berg and Kaj Nyström. A unified deep artificial neural network approach to partial differential equations in complex geometries. *Neurocomputing*, 317:28–41, 2018.
- [2] Ilia Binder and Mark Braverman. The rate of convergence of the Walk on Spheres algorithm. *Geometric and Functional Analysis*, 22(3):558–587, 2012. doi: 10.1007/s00039-012-0161-z.
- [3] Mario Botsch, Leif Kobbelt, Mark Pauly, Pierre Alliez, and Bruno Lévy. *Polygon Mesh Processing*. CRC Press, 2010.
- [4] Susanne Brenner and Ridgway Scott. *The Mathematical Theory of Finite Element Methods*. Springer, 3rd edition, 2008.
- [5] William L. Briggs, Van Emden Henson, and Steve F. McCormick. *A Multigrid Tutorial*. SIAM, 2nd edition, 2000.
- [6] Keenan Crane, Fernando de Goes, Mathieu Desbrun, and Peter Schröder. Digital geometry processing with discrete exterior calculus. *ACM SIGGRAPH 2013 Courses*, 2013.
- [7] Salvatore Cuomo, Vincenzo Schiano Di Cola, Fabio Giampaolo, Gianluigi Rozza, Maziar Raissi, and Francesco Piccialli. Scientific machine learning through physics-informed neural networks: Where we are and what’s next. *Journal of Scientific Computing*, 92(3):88, 2022.
- [8] Jia Deng, Wei Dong, Richard Socher, Li-Jia Li, Kai Li, and Li Fei-Fei. ImageNet: A large-scale hierarchical image database. In *2009 IEEE Conference on Computer Vision and Pattern Recognition*, pages 248–255. IEEE, 2009. doi: 10.1109/CVPR.2009.5206848.
- [9] David Donoho. Data science at the singularity. *Harvard Data Science Review*, 6(1), 2024. doi: 10.1162/99608f92.b91339ef.
- [10] Chi-Mao Fan, Tsung-Jung Liu, and Kuan-Hsien Liu. SUNet: Swin transformer UNet for image denoising. In *2022 IEEE International Symposium on Circuits and Systems (ISCAS)*. IEEE, May 2022. doi: 10.1109/iscas48785.2022.9937486.
- [11] Stuart Geman, Elfe Bienenstock, and René Doursat. Neural networks and the bias/variance dilemma. *Neural Computation*, 4(1):1–58, 1992.
- [12] Jayesh K. Gupta and Johannes Brandstetter. Towards multi-spatiotemporal-scale generalized pde modeling. *arXiv preprint arXiv:2209.15616*, 2022.
- [13] Trevor Hastie, Robert Tibshirani, and Jerome Friedman. *The Elements of Statistical Learning: Data Mining, Inference, and Prediction*. Springer, 2 edition, 2009.
- [14] Maximilian Herde, Nils Wandel, Siddhartha Mishra, Nils Thuerey, and Bogdan Raonic. Poseidon: Efficient foundation models for pdes. In *Advances in Neural Information Processing Systems*, 2024.
- [15] Masanobu Horie and Naoto Mitsume. Physics-embedded neural networks: Graph neural pde solvers with mixed boundary conditions. In *Advances in Neural Information Processing Systems*, volume 35, pages 23218–23229. Curran Associates, Inc., 2022.
- [16] Jiahe Huang, Guandao Yang, Zichen Wang, and Jeong Joon Park. Diffusionpde: Generative pde-solving under partial observation. *Advances in Neural Information Processing Systems*, 37: 130291–130323, 2024.
- [17] Christian Jacobsen, Yilin Zhuang, and Karthik Duraisamy. Cocogen: Physically consistent and conditioned score-based generative models for forward and inverse problems. *SIAM Journal on Scientific Computing*, 2024.
- [18] Zichao Jiang, Junyang Jiang, Qinghe Yao, and Gengchao Yang. A neural network-based pde solving algorithm with high precision. *Scientific Reports*, 13(1):4479, 2023.
- [19] Guoliang Jin, Lin Chen, and Jiamei Dong. Monte carlo finite element method of structure reliability analysis. *Reliability Engineering & System Safety*, 40(1), 1993. doi: 10.1016/0951-8320(93)90121-E.

- [20] Bahjat Kawar, Michael Elad, Stefano Ermon, and Jiaming Song. Denoising diffusion restoration models. In *Advances in Neural Information Processing Systems*, volume 35, pages 23593–23606, 2022.
- [21] Yuehaw Khoo, Jianfeng Lu, and Lexing Ying. Solving parametric pde problems with artificial neural networks. *European Journal of Applied Mathematics*, 32(3):421–435, 2021.
- [22] Erich L Lehmann and George Casella. *Theory of Point Estimation*. Springer, 2 edition, 1998.
- [23] Zilu Li, Guandao Yang, Xi Deng, Christopher De Sa, Bharath Hariharan, and Steve Marschner. Neural caches for monte carlo partial differential equation solvers. In *SIGGRAPH Asia 2023 Conference Papers*, SA '23. Association for Computing Machinery, 2023. doi: 10.1145/3610548.3618141.
- [24] Zongyi Li, Nikola Borislavov Kovachki, Kamyar Azizzadenesheli, Burigede liu, Kaushik Bhattacharya, Andrew Stuart, and Anima Anandkumar. Fourier neural operator for parametric partial differential equations. In *International Conference on Learning Representations*, 2021. URL <https://openreview.net/forum?id=c8P9NQVtmn0>.
- [25] Zongyi Li, Hongkai Zheng, Nikola B. Kovachki, David Jin, Haoxuan Chen, Burigede Liu, Kamyar Azizzadenesheli, and Anima Anandkumar. Physics-informed neural operator for learning partial differential equations. *CoRR*, abs/2111.03794, 2021. URL <https://arxiv.org/abs/2111.03794>.
- [26] Michael Mascagni and Chi-Ok Hwang. ϵ -Shell error analysis for “Walk On Spheres” algorithms. *Mathematics and Computers in Simulation*, 63(2):93–104, 2003. doi: 10.1016/S0378-4754(03)00038-7.
- [27] M. Muller. Some continuous monte carlo methods for the dirichlet problem. *Ann. Math. Statist.*, 27(3), 1956.
- [28] Maziar Raissi, Paris Perdikaris, and George Em Karniadakis. Physics informed deep learning (part i): Data-driven solutions of nonlinear partial differential equations, 2017.
- [29] Pratik Rathore, Weimu Lei, Zachary Frangella, Lu Lu, and Madeleine Udell. Challenges in training PINNs: A loss landscape perspective, 2024.
- [30] Rohan Sawhney and Keenan Crane. Monte carlo geometry processing: A grid-free approach to pde-based methods on volumetric domains. *ACM Trans. Graph.*, 39(4), 2020.
- [31] Rohan Sawhney, Dario Seyb, Wojciech Jarosz, and Keenan Crane. Grid-free monte carlo for pdes with spatially varying coefficients. *ACM Trans. Graph.*, 41(4), July 2022. ISSN 0730-0301. doi: 10.1145/3528223.3530134.
- [32] Rohan Sawhney, Dario Seyb, Wojciech Jarosz, and Keenan Crane. Walk on stars: A grid-free monte carlo method for pdes with neumann boundary conditions. *ACM Trans. Graph.*, 2023.
- [33] Ryusuke Sugimoto, Terry Chen, Yiti Jiang, Christopher Batty, and Toshiya Hachisuka. A practical walk-on-boundary method for boundary value problems. *ACM Transactions on Graphics*, 42(4):1–16, July 2023. ISSN 1557-7368. doi: 10.1145/3592109.
- [34] Makoto Takamoto, Timothy Praditia, Raphael Leiteritz, Daniel MacKinlay, Francesco Alesiani, Dirk Pflüger, and Mathias Niepert. Pdebench: An extensive benchmark for scientific machine learning. In *NeurIPS Datasets and Benchmarks Track*, 2022.
- [35] Alex Wang, Amanpreet Singh, Julian Michael, Felix Hill, Omer Levy, and Samuel Bowman. GLUE: A multi-task benchmark and analysis platform for natural language understanding. In *Proceedings of the 2018 EMNLP Workshop BlackboxNLP: Analyzing and Interpreting Neural Networks for NLP*, pages 353–355, Brussels, Belgium, 2018. Association for Computational Linguistics. doi: 10.18653/v1/W18-5446. URL <https://aclanthology.org/W18-5446>.
- [36] Alex Wang, Yada Pruksachatkun, Nikita Nangia, Amanpreet Singh, Julian Michael, Felix Hill, Omer Levy, and Samuel R. Bowman. SuperGLUE: A stickier benchmark for general-purpose language understanding systems. In *Advances in Neural Information Processing Systems*, volume 32, 2019.

- [37] Sifan Wang, Xinling Yu, and Paris Perdikaris. When and why pinns fail to train: A neural tangent kernel perspective. *Journal of Computational Physics*, 449:110768, 2022.
- [38] Rui Zhang, Qi Meng, Rongchan Zhu, Yue Wang, Wenlei Shi, Shihua Zhang, Zhi-Ming Ma, and Tie-Yan Liu. Monte carlo neural pde solver for learning pdes via probabilistic representation, 2023.

A PDEZoo: Detailed Specifications

A.1 Solution Atom Types

Each solution $u(x, y)$ is constructed as a sum of n randomly chosen atoms, where n is sampled uniformly from $[2, 6]$. For Poisson and Yukawa instances, atoms are drawn from the **general pool** (20 types); for Laplace instances, atoms are drawn from the **harmonic pool** (12 unique types). For Poisson and Yukawa instances, atoms are drawn from a pool of 20 such types. For Laplace instances, atoms are restricted to a pool of 12 analytically harmonic types — real and imaginary parts of holomorphic functions such as z^n , e^{kz} , $\log(z - z_0)$, and $1/(z - z_0)^n$ — guaranteeing $\nabla^2 h = 0$ by construction. High-frequency and sharp-featured atoms are deliberately over-represented to produce instances where Monte Carlo variance is large and correction is non-trivial, yielding a calibrated difficulty distribution (Appendix A.1). Combinatorially, choosing 2–6 atoms from these pools yields over 60,000 distinct type tuples for Poisson/Yukawa alone; each tuple is further parameterized by continuous amplitudes, frequencies, and source locations, making the effective solution space inexhaustible.

General atoms (Poisson/Yukawa). Table 4 lists all 20 general atom types. Five of these are designated as *hard atoms* (marked with †), producing high-frequency oscillations, narrow features, or sharp transitions that increase Monte Carlo variance. Hard atoms are over-represented in the selection pool via the `hard_atom_extra` parameter (set to 4), which appends 4 extra copies of each hard atom, raising their draw probability from 25% to 63%.

Table 4: General atom types for Poisson and Yukawa instances. † = hard atom.

Atom	Form	Key Parameters
poly	Polynomial (degree ≤ 3)	Coefficients in $[-1, 1]$
trig	$a \sin(k\pi x)$	$k \in [1, 6]$
exp	$a \exp(bx)$	$b \in [-2, 2]$
log	$a \log(x^2 + 0.01)$	—
hyper	$a \sinh / \cosh / \tanh(x)$	—
special	$a \operatorname{erf}(x)$ or $a\sqrt{x^2 + \varepsilon}$	—
harmonic_polar	$ar^n \cos(n\theta)$	$n \in [1, 6]$
plane_wave	$a \cos(k\hat{n} \cdot x)$	$k \in [1, 8]$
yukawa_i0	$a I_0(\mu r)$	μ from $\lambda \in [0.5, 6]$
log_source	$a \log x - x_0 $	$\rho \in [1.8, 2.5]$
gaussian_bump	$a \exp(-w \ x - x_0\ ^2)$	$w \in [0.8, 2]$
rational	$a / (1 + bx^2 + cy^2)$	$b, c \in [0.5, 3]$
product	$a f_1(k_1 x) f_2(k_2 y)$	$f_i \in \{\sin, \cos, \tanh\}$
multi_rbf	Sum of 2–4 Gaussians	$w \in [2, 8]$
high_freq_trig†	$a \sin(k_1 \pi x) \cos(k_2 \pi y)$	$k_1, k_2 \in [2, 8]$
logsumexp	$a \operatorname{logaddexp}(bx, cy)$	$b, c \in [1, 4]$
sech_bump†	$a / (\cosh^2 b(x - x_0) \cosh^2 c(y - y_0))$	$b, c \in [2, 6]$
very_high_freq_trig†	$a \sin(k_1 \pi x) \cos(k_2 \pi y)$	$k_1, k_2 \in [6, 15]$
narrow_bump†	$a \exp(-w \ x - x_0\ ^2)$	$w \in [8, 25]$
sharp_transition†	$a \tanh(k(\hat{n} \cdot x - c))$	$k \in [5, 15]$

Harmonic atoms (Laplace). Table 5 lists the 12 unique harmonic atom types. Every harmonic atom is the real or imaginary part of a holomorphic function $f(z)$ where $z = x + iy$, guaranteeing $\nabla^2 h = 0$ analytically by the Cauchy–Riemann equations. Two types (marked †) constitute the hard harmonic atoms, producing solutions with high spatial frequency or signal concentrated near the boundary.

Table 5: Harmonic atom types for Laplace instances. † = hard atom. Weight indicates the number of entries in the base selection pool.

Atom	Form	Complex Origin	Wt.
h_polar	$ar^n \cos / \sin(n\theta)$	Re/Im(z^n), $n \in [1, 6]$	2
h_exp_trig	$ae^{kx} \cos / \sin(ky)$	Re/Im(e^{kz}), $k \in [-3, 3]$	2
h_trig_hyp	$a \sin(kx) \sinh(ky)$ etc.	Separable, $k \in [0.5, 4]$	2
h_log_source	$a \log x - x_0 $	Re($\log(z - z_0)$), $\rho \geq 1.8$	2
h_linear	$ax + by$	Re(αz)	1
h_bilinear	axy	Im(z^2)/2	1
h_arctan	$a \operatorname{atan2}(y - y_0, x - x_0)$	Im($\log(z - z_0)$)	1
h_inversion	$a(x - x_0)/ x - x_0 ^2$	Re($1/(z - z_0)$)	1
h_dipole	$a(\Delta x^2 - \Delta y^2)/ \Delta ^4$	Re($1/(z - z_0)^2$)	1
h_quadratic	$a(u^2 - v^2)$ or $2uv$	Re/Im(z^2) rotated	2
h_high_freq_exp_trig†	$ae^{kx} \cos / \sin(ky)$	Re/Im(e^{kz}), $k \in [4, 10]$	2
h_high_n_polar†	$ar^n \cos / \sin(n\theta)$	Re/Im(z^n), $n \in [6, 12]$	2

A.2 Domain Geometry

PDEZoo includes 8 primitive domain families and composed domains. All domains are centered approximately at the origin; the evaluation grid spans $[-1, 1]^2$. Each primitive has probability $1/11$ of being selected; composed domains have combined probability $3/11$.

Table 6: Primitive domain types with parameter ranges and SDF properties.

Domain	Key Parameters	SDF	Exact?
Disk	$R = 1.0$	$R - x $	Yes
Square	half = 1.0	$\min(\text{half} - x_i)$	Yes
Rectangle	$a, b \in [0.6, 1.2]$	$\min(a - x , b - y)$	Yes
Ellipse	$r_x, r_y \in [0.6, 1.2]$	$(1 - x/r) \min(r_x, r_y)$	Approx.
Annulus	$r_{\text{in}} \in [0.2, 0.6], r_{\text{out}} \in [0.8, 1.4]$	$\min(r_{\text{out}} - r, r - r_{\text{in}})$	Yes
Triangle	Equilateral, $R \in [0.6, 1.0]$	$\min(\text{signed edge dists})$	Yes
Hexagon	Regular, $R \in [0.6, 1.0]$	$\min(\text{signed edge dists})$	Yes
Stadium	half_len $\in [0.2, 0.6], \text{rad} \in [0.25, 0.5]$	rad - dist to segment	Yes

Composed domains. Composed domains combine two randomly selected primitives (from disk, rectangle, ellipse, or triangle) via a Boolean operation: union ($3/7$), intersection ($2/7$), or difference ($2/7$). Each component has independent random parameters, rotation, and offset (separation $\in [0.15, 0.55]$). The composed SDF is computed as $\max(\text{sdf}_A, \text{sdf}_B)$ for union, $\min(\text{sdf}_A, \text{sdf}_B)$ for intersection, and $\min(\text{sdf}_A, -\text{sdf}_B)$ for difference. These are provably conservative (i.e., $\text{sdf}(x) \leq \text{dist}(x, \partial\Omega)$), ensuring every WoS ball lies entirely within Ω .

A.3 Quality Filters

Each generated instance must pass eight quality filters before inclusion (up to 40 retries per case):

Table 7: Quality filters applied during case generation.

Filter	Condition
Finite test point	$u(0.3, 0.4)$ is finite
Finite forcing	$f(0.3, 0.4)$ is finite (Poisson/Yukawa only)
Domain interior	≥ 10 interior points in 128 random samples
Composed thickness	Median SDF > 0.03 over interior points
Solution amplitude	$10^{-3} < \text{std}(u) < 200$
Boundary values	$\max u(\partial\Omega) < 500$ (composed only)
Forcing amplitude	$10^{-4} < \text{std}(f) < 500$ (Poisson/Yukawa only)
Finite ground truth	All GT values inside domain are finite at 256×256

The WoS solver uses boundary termination threshold $\varepsilon = 10^{-4}$, introducing bias bounded by $|\text{bias}| \lesssim 10^{-3} \|g\|_\infty$ [2] — negligible compared to MC variance at all practical budgets. For each

Table 8: Difficulty tier definitions and observed distribution ($B = 32$).

Tier	MSE @ $B = 32$	Typical Characteristics	Proportion
Easy	$< 10^{-2}$	Smooth, low-frequency, simple domains	$\sim 20\%$
Medium	$[10^{-2}, 1)$	Moderate frequency, diverse domains	$\sim 41\%$
Hard	$[1, 10^2)$	High-freq. oscillations, strong sources	$\sim 30\%$
Very Hard	$\geq 10^2$	Very high-freq. patterns, sharp features	$\sim 8\%$

instance, PDEZoo also provides an executable description of u (and hence f, g) and geometry accessors (SDF evaluator, boundary projection, samplers).

A.4 Data Format

Each instance is stored as a JSONL record containing: case ID, PDE kind (`laplace`, `poisson`, or `yukawa`), screening parameter λ (nonzero only for Yukawa), a PyTorch expression string for the analytic solution, domain name and parameters, number of atom terms, and hardness metadata (`std(u)`, `std(f)`).

Each packaged `.npz` file contains three (256×256) float32 arrays:

- `noisy`: MC solution at the given budget (0.0 outside domain)
- `clean`: Ground truth analytic solution (0.0 outside domain)
- `mask`: Domain indicator (1.0 inside, 0.0 outside)

A.5 Convergence Verification

We verify empirically that the WoS estimator achieves the theoretical $\mathcal{O}(1/N)$ MSE convergence rate by fitting log-log MSE slopes over budgets 1–32 across 501 test cases (167 per PDE type). Table 9 reports the results: the median slope is exactly -1.000 for all three families, and 99.6% of cases fall within $[-1.05, -0.95]$. This confirms that the manufactured solutions, derived forcing functions, and WoS implementation are mutually consistent. Convergence verification results are presented in Table 9 in the main text. The MSE of the WoS estimator satisfies $\text{MSE}(N) = \text{Var}(\text{single walk})/N = \mathcal{O}(1/N)$. On a log-log plot, this yields slope -1.0 regardless of PDE type, domain geometry, solution difficulty, or Yukawa screening strength λ ; difficulty affects only the constant (variance per walk), not the rate. Very Hard cases are almost exclusively Laplace, because the Yukawa screening weight $\psi = 1/I_0(\mu R)$ exponentially damps estimator variance.

A.6 Difficulty Distribution

Difficulty tier definitions and the observed distribution are presented in Table 8 in the main text. The difficulty distribution was calibrated via a 12-configuration hyperparameter sweep varying hard-atom weighting, term count ranges, and amplitude filter caps. The selected configuration (`hard_atom_extra = 4`) shifts the distribution from a baseline of (34/45/17/4)% to the target (20/41/30/8)%, ensuring sufficient representation of challenging instances.

A.7 PDEZoo

Each PDE instance is defined by a tuple $\mathcal{P} = (\Omega, \mathcal{E}, f, g, u)$ where $\Omega \subset \mathbb{R}^d$ is a bounded domain with boundary $\partial\Omega$, \mathcal{E} denotes an elliptic PDE family, $f : \Omega \rightarrow \mathbb{R}$ is a forcing term, $g : \partial\Omega \rightarrow \mathbb{R}$ specifies Dirichlet boundary condition, and $u : \Omega \rightarrow \mathbb{R}$ is the analytical solution. PDEZoo includes five elliptic PDE families:

Laplace. The solution satisfies $\Delta u = 0$ in Ω , with Dirichlet boundary condition $u = g$ on $\partial\Omega$. In this setting, u is constructed from analytically harmonic atoms.

Poisson. The solution satisfies $\Delta u = f$ in Ω , with Dirichlet boundary values inherited from the manufactured solution. Here, u is sampled from a rich family of smooth non-harmonic expressions, and the source term is obtained as $f = \Delta u$.

Table 9: Empirical WoS convergence slope verification on 501 test cases. The theoretical rate is slope = -1.0 .

PDE Type	Median Slope	Min	Max	% in $[-1.05, -0.95]$
Laplace	-1.000	-1.015	-0.981	100.0%
Poisson	-1.000	-1.045	-0.918	99.4%
Yukawa	-1.000	-1.043	-0.944	99.4%
All	-1.000	-1.045	-0.918	99.6%

Yukawa. The solution satisfies $\Delta u - \lambda u = f$ in Ω , with screening parameter $\lambda > 0$. The source is defined from the manufactured solution by $f = \Delta u - \lambda u$. In our dataset, λ is sampled uniformly from $[0.5, 50.0]$.

Biharmonic. The solution satisfies $\Delta^2 u = f$ in Ω , with Dirichlet boundary condition $u = g$ on $\partial\Omega$. Here, u is sampled from a family of smooth manufactured expressions, and the source term is obtained as $f = \Delta^2 u$, where $\Delta^2 = \Delta(\Delta \cdot)$ denotes the biharmonic operator.

Helmholtz. The solution satisfies $\Delta u + k^2 u = f$ in Ω , with wavenumber $k > 0$ and Dirichlet boundary values inherited from the manufactured solution. The source is defined as $f = \Delta u + k^2 u$. In our dataset, k is sampled uniformly from $[0.5, 10.0]$.

B Monte Carlo Walk-On-Spheres Solver

B.1 WoS Solver Parameters

The Walk-on-Spheres solver uses the following parameters:

Table 10: WoS solver parameters.

Parameter	Value	Description
Resolution	256×256	Uniform grid over $[-1, 1]^2$
ε (shell)	10^{-4}	Boundary termination threshold
max_steps (train)	128	Maximum walk steps per sample
max_steps (eval)	256	Higher for convergence verification
walk_batch	256	Walks processed per GPU batch

ε -shell bias. The WoS walk terminates when the signed distance to $\partial\Omega$ falls below $\varepsilon = 10^{-4}$, introducing a bias bounded by $|E[\hat{u}(x)] - u(x)| \leq C\varepsilon |\log \varepsilon| \cdot \|g\|_\infty$ for 2D Laplace with Hölder-continuous boundary data [2]. At $\varepsilon = 10^{-4}$ this gives $|\text{bias}| \lesssim 10^{-3} \|g\|_\infty$, negligible compared to the MC standard deviation σ/\sqrt{N} at all practical budgets.

C MC² Architecture

Our MC² corrector is instantiated as a Swin-UNet (SUNet) architecture [10]. The model processes 256×256 inputs with patch size 4, embedding dimension 96, and four encoder stages with depths $[8, 8, 8, 8]$ and $[8, 8, 8, 8]$ attention heads. The decoder mirrors the encoder with skip connections. We use a window size of 8 for shifted-window self-attention, MLP ratio 4, and stochastic depth with drop path rate 0.1. The final layer uses dual upsampling to reconstruct the full-resolution output. We then train for 200 epochs using the AdamW optimizer with initial learning rate 2×10^{-4} (decaying to 10^{-6}), batch size 48, and bf16 mixed precision. Training is distributed across 4 GPUs using PyTorch’s DDP. The loss function is mean squared error (MSE) between predicted and ground truth solutions, computed only on valid interior regions as defined by the domain mask. We select the checkpoint with the best validation PSNR.

D Baseline Models

D.1 Denoisers

For traditional denoisers, we utilize Gaussian filtering ($\sigma = 1.0$), heavy Gaussian filtering ($\sigma = 2.0$), Median filtering (disk radius 2), Bilateral filtering ($\sigma_{\text{color}} = 0.1$, $\sigma_{\text{spatial}} = 5$), Total Variation minimization (weight 0.1), and Non-Local Means (patch size 5, search distance 6, $h = 0.1$).

D.2 FNO

The architecture uses 4 Fourier layers with 16 modes and width 64. We train for 200 epochs using Adam with learning rate 10^{-3} , batch size 16 per GPU across 4 GPUs, and StepLR scheduling (step size 100, $\gamma = 0.5$).

E Extended Results

E.1 Full Per-Family Results

For completeness, Table 11 reports per-family results across all four metrics (PSNR, SNR, MSE, LPIPS) for every method evaluated in the main paper, including the full Walk-on-Spheres compute curve from $B = 8$ to $B = 131,072$. The aggregate trends mirror the main-paper findings: MC^2 from a single $B = 8$ WoS input matches WoS quality at $B \sim 16,384\text{--}32,768$ on in-distribution families and at $B \sim 8,192\text{--}16,384$ on out-of-distribution families, corresponding to a $1,024\text{--}4,096\times$ reduction in Monte Carlo compute. The per-family breakdown also reveals where each baseline method’s weaknesses concentrate. PINO’s physics regularization actively harms performance on every family, producing solutions worse than the raw $B = 8$ input. Diffusion-based methods (CoCoGen, DiffusionPDE) achieve reasonable Laplace performance but degrade sharply on Poisson and Yukawa, where forcing-driven structure is harder to capture from generative priors alone. FNO is the strongest baseline overall but trails MC^2 by 13–16 dB on every family. Among traditional denoisers, Non-Local Means and Total Variation provide the largest gains over raw WoS, but plateau well below the neural methods. LPIPS values reinforce the PSNR ranking: MC^2 is the only method that achieves perceptually-near-zero error (< 0.02) on every family.

Table 11: Full per-family results across all four metrics on the PDEZoo test set. PSNR and SNR are reported in dB; MSE and LPIPS are unitless. Arrows indicate metric direction. **B**bold marks the best result per column among learned and post-processing methods. MC^2 uses a single $B = 8$ WoS input.

METHOD	LAPLACE				POISSON				YUKAWA				BIHARMONIC				HELMHOLTZ				OVERALL			
	PSNR†	SNR†	MSE↓	LPIPS↓	PSNR†	SNR†	MSE↓	LPIPS↓	PSNR†	SNR†	MSE↓	LPIPS↓	PSNR†	SNR†	MSE↓	LPIPS↓	PSNR†	SNR†	MSE↓	LPIPS↓	PSNR†	SNR†	MSE↓	LPIPS↓
<i>Walk-on-Spheres (Monte Carlo)</i>																								
WOS ($B=8$)	25.22	19.17	4.02e-03	0.5188	11.20	5.90	0.1214	0.8220	13.89	8.48	0.0793	0.7298	15.01	9.65	0.0716	0.7315	10.93	5.60	0.1247	0.8360	15.26	9.77	0.0802	0.7275
WOS ($B=16$)	28.22	22.17	2.07e-03	0.4377	12.41	7.11	0.1086	0.7957	15.56	10.15	0.0652	0.6886	16.61	11.25	0.0665	0.6958	12.06	6.73	0.1126	0.8131	16.99	11.50	0.0710	0.6861
WOS ($B=32$)	31.21	25.17	1.06e-03	0.3561	13.89	8.59	0.0936	0.7627	17.50	12.09	0.0511	0.6416	18.42	13.05	0.0603	0.6553	13.48	8.14	0.0982	0.7831	18.91	13.42	0.0609	0.6396
WOS ($B=64$)	34.22	28.17	5.35e-04	0.2782	15.63	10.33	0.0777	0.7229	19.67	14.26	0.0383	0.5901	20.40	15.04	0.0533	0.6107	15.15	9.82	0.0828	0.7451	21.03	15.54	0.0506	0.5893
WOS ($B=128$)	37.23	31.18	2.70e-04	0.2090	17.60	12.30	0.0622	0.6772	22.05	16.64	0.0273	0.5336	22.54	17.18	0.0457	0.5640	17.06	11.73	0.0674	0.7015	23.31	17.82	0.0407	0.5370
WOS ($B=256$)	40.23	34.19	1.35e-04	0.1520	19.78	14.47	0.0479	0.6273	24.60	19.19	0.0185	0.4725	24.82	19.46	0.0381	0.5161	19.18	13.85	0.0530	0.6529	25.74	20.24	0.0316	0.4841
WOS ($B=512$)	43.25	37.20	6.78e-05	0.1065	22.13	16.83	0.0353	0.5733	27.28	21.87	0.0119	0.4094	27.21	21.85	0.0306	0.4676	21.49	16.16	0.0402	0.6005	28.29	22.79	0.0237	0.4315
WOS ($B=1024$)	46.26	40.21	3.39e-05	0.0700	24.65	19.35	0.0248	0.5161	30.07	24.66	7.28e-03	0.3489	29.68	24.31	0.0238	0.4199	23.95	18.62	0.0294	0.5446	30.94	25.44	0.0171	0.3800
WOS ($B=2048$)	49.27	43.22	1.70e-05	0.0419	27.31	22.01	0.0165	0.4560	32.95	27.54	4.25e-03	0.2924	32.20	26.84	0.0178	0.3717	26.56	21.22	0.0206	0.4866	33.67	28.17	0.0119	0.3299
WOS ($B=4096$)	52.27	46.23	8.49e-06	0.0228	30.08	24.78	0.0104	0.3954	35.87	30.46	2.38e-03	0.2399	34.77	29.40	0.0127	0.3241	29.26	23.93	0.0138	0.4270	36.46	30.97	7.91e-03	0.2820
WOS ($B=8192$)	55.29	49.24	4.25e-06	0.0111	32.94	27.64	6.26e-03	0.3367	38.83	33.42	1.28e-03	0.1902	37.30	31.93	8.75e-03	0.2799	32.05	26.72	8.91e-03	0.3681	39.29	33.80	5.07e-03	0.2375
WOS ($B=16384$)	58.30	52.25	2.12e-06	0.0049	35.86	30.55	3.57e-03	0.2824	41.81	36.41	6.73e-04	0.1431	39.77	34.41	5.84e-03	0.2384	34.89	29.56	5.49e-03	0.3115	42.14	36.64	3.13e-03	0.1964
WOS ($B=32768$)	61.31	55.26	1.06e-06	0.0019	38.81	33.51	1.96e-03	0.2329	44.80	39.39	3.45e-04	0.1066	42.15	36.79	3.80e-03	0.2004	37.77	32.44	3.25e-03	0.2583	44.98	39.49	1.88e-03	0.1592
WOS ($B=65536$)	64.31	58.27	5.31e-07	0.0007	41.78	36.47	1.04e-03	0.1874	47.79	42.38	1.75e-04	0.0654	44.40	39.03	2.44e-03	0.1656	40.67	35.34	1.87e-03	0.2102	47.80	42.31	1.11e-03	0.1263
WOS ($B=131072$)	67.32	61.27	2.66e-07	0.0003	44.77	39.47	5.40e-04	0.1442	50.80	45.38	8.83e-05	0.0390	46.49	41.13	1.57e-03	0.1347	43.56	38.23	1.06e-03	0.1669	50.60	45.10	6.56e-04	0.0974
<i>Traditional Denoisers (applied to $B=8$ WoS)</i>																								
GAUSSIAN	23.40	17.64	1.26e-03	0.5022	13.68	8.25	0.0892	0.5106	17.46	11.92	0.0420	0.3827	17.62	12.22	0.0589	0.3988	14.26	9.02	0.0334	0.4658	17.28	11.95	0.0561	0.4543
GAUSSIAN (HEAVY)	25.92	20.23	3.25e-04	0.1788	13.87	8.44	0.1052	0.3766	16.96	10.76	0.0673	0.2965	16.10	10.62	0.0303	0.3326	14.19	8.92	0.0840	0.3440	17.74	11.77	0.0446	0.2964
TOTAL VARIATION	37.98	32.29	1.86e-04	0.1329	18.16	12.85	0.0651	0.3987	23.50	17.96	0.0182	0.3145	23.24	17.84	0.0318	0.2777	18.84	13.60	0.0488	0.3561	24.34	18.74	0.0258	0.2787
NON-LOCAL MEANS	39.60	33.91	1.34e-04	0.1004	20.49	15.06	0.0374	0.4956	23.96	18.35	0.0117	0.3032	25.20	19.80	0.0265	0.3394	21.06	15.82	0.0352	0.4624	26.27	20.82	0.0227	0.3390
<i>Neural Network Methods</i>																								
FNO	44.06	38.17	6.05e-05	0.0106	24.26	18.83	0.0237	0.3394	29.58	24.14	7.15e-03	0.1801	29.43	24.03	0.0223	0.2624	24.50	19.06	0.0237	0.2988	30.34	24.89	0.0159	0.2196
PINO	18.50	12.61	0.0499	0.1894	6.18	3.83	0.2724	0.4210	8.26	2.81	0.2441	0.3832	5.69	0.30	3.0077	0.3476	5.89	0.65	0.2934	0.4515	7.68	2.23	0.2585	0.3886
CoCoGen	23.98	18.22	4.85e-03	0.6184	11.11	5.86	0.1265	0.8495	14.87	9.12	0.0686	0.6474	-	-	-	-	-	-	-	16.95	11.41	0.0532	0.6982	
DIFFUSIONPDE	24.77	19.00	4.16e-03	0.6519	11.11	5.88	0.1266	0.8495	14.67	9.11	0.0686	0.6475	-	-	-	-	-	-	-	17.23	11.68	0.0529	0.6958	
MC^2 (OURS)	60.21	54.52	2.53e-06	0.0001	40.80	35.37	6.39e-04	0.0085	46.83	41.08	1.83e-05	0.0016	34.88	29.48	9.15e-05	0.0785	35.87	34.64	1.15e-03	0.0091	44.10	38.05	2.37e-03	0.0208

F Bias–Variance Analysis of PDE Solvers

Here, we formalize the bias–variance tradeoff among three estimators of an elliptic PDE solution u : the pure Monte Carlo Walk-on-Spheres estimator \hat{u}_K , a pure neural operator Φ_θ^{DP} , and our hybrid MC^2 estimator $\tilde{u}_K = \Phi_\theta(\hat{u}_K, a)$, where a denotes any auxiliary conditioning information available to

Table 12: Effect of training data scale on MC² performance. All models use $B = 8$ WoS inputs. Fractions denote the proportion of the full training set used.

Data fraction	Biharmonic				Helmholtz				Laplace				Poisson				Yukawa				Overall			
	PSNR \uparrow	SNR \uparrow	MSE \downarrow	LPIPS \downarrow	PSNR \uparrow	SNR \uparrow	MSE \downarrow	LPIPS \downarrow	PSNR \uparrow	SNR \uparrow	MSE \downarrow	LPIPS \downarrow	PSNR \uparrow	SNR \uparrow	MSE \downarrow	LPIPS \downarrow	PSNR \uparrow	SNR \uparrow	MSE \downarrow	LPIPS \downarrow	PSNR \uparrow	SNR \uparrow	MSE \downarrow	LPIPS \downarrow
0.04 \times	31.68	26.276	0.0127	0.1970	30.72	25.310	5.74e-03	0.2386	50.65	44.657	1.26e-05	0.0058	31.07	25.712	3.84e-03	0.2401	35.41	29.994	1.26e-03	0.1088	35.79	30.278	4.84e-03	0.1594
0.08 \times	33.51	28.102	0.0110	0.1534	34.66	29.257	3.03e-03	0.1358	53.76	47.767	6.19e-06	0.0014	35.07	29.709	1.77e-03	0.1285	39.53	34.114	5.13e-04	0.0391	39.18	33.663	3.37e-03	0.0929
0.16 \times	33.96	28.555	0.0117	0.1268	35.32	29.908	3.31e-03	0.0814	54.70	48.716	5.09e-06	0.0006	35.92	30.555	1.61e-03	0.0714	40.30	34.886	5.36e-04	0.0178	39.91	34.392	5.54e-03	0.0607
0.32 \times	35.41	30.003	8.79e-03	0.1333	35.95	30.538	3.14e-03	0.1130	55.32	49.330	4.33e-06	0.0005	36.42	31.060	1.71e-03	0.0877	40.58	35.166	5.39e-04	0.0238	40.61	35.097	2.92e-03	0.0729
0.64 \times	35.77	30.363	8.57e-03	0.0826	38.96	33.556	1.41e-03	0.0183	58.62	52.629	2.18e-06	0.0001	40.14	34.781	6.05e-04	0.0119	44.63	39.209	1.49e-04	0.0027	43.47	37.952	2.23e-03	0.0239
1.0 \times (full)	35.74	30.332	7.51e-03	0.0628	40.29	34.878	1.13e-03	0.0108	59.76	53.772	1.80e-06	0.0001	41.63	36.272	4.70e-04	0.0054	45.86	40.440	1.58e-04	0.0016	44.48	38.972	1.92e-03	0.0167

the corrector, such as the source term, domain mask, boundary data, or PDE parameters. Throughout, we use the standard bias–variance decomposition of mean-squared error under squared loss [11, 13]. We present the analysis pointwise at a fixed query $x \in \Omega$; the same conclusions hold for discretized fields by summing over grid points, or in $L^2(\Omega)$ by integration. For an estimator T of $u(x)$, the conditional mean-squared error decomposes as

$$\mathbb{E}[(T - u(x))^2 | P] = \underbrace{(\mathbb{E}[T | P] - u(x))^2}_{\text{Bias}^2(T|P)} + \underbrace{\text{Var}(T | P)}_{\text{Variance}(T|P)}, \quad (3)$$

where P denotes the underlying PDE instance and the expectation is over the internal randomness of the estimator.

F.1 Monte Carlo WoS Solver

Let $\hat{u}_K(x) = \frac{1}{K} \sum_{k=1}^K Y_k(x)$ be the WoS estimator using K independent walks per query point. WoS expresses the solution of elliptic boundary-value problems as the expectation of a random variable induced by Green’s functions and boundary hitting distributions [27, 30]. Thus, ignoring the small ε -shell termination bias,

$$\mathbb{E}[\hat{u}_K(x) | P] = u(x). \quad (4)$$

With ε -shell termination, the estimator has a small boundary bias that decays linearly in ε with rate depending on local geometry [26, 2]:

$$|\mathbb{E}[\hat{u}_K(x) | P] - u(x)| = \mathcal{O}(\varepsilon). \quad (5)$$

The variance of the average of K independent walks is

$$\text{Var}(\hat{u}_K(x) | P) = \frac{\sigma_P^2(x)}{K}, \quad (6)$$

where $\sigma_P^2(x) = \text{Var}(Y_1(x) | P)$ is the single-walk variance. Therefore,

$$\mathbb{E}[(\hat{u}_K(x) - u(x))^2 | P] = \frac{\sigma_P^2(x)}{K} + \mathcal{O}(\varepsilon^2). \quad (7)$$

Thus, pure WoS is approximately unbiased, but its variance decays only as $\mathcal{O}(1/K)$.

F.2 Neural Operators

A pure neural operator maps a PDE specification directly to a solution field, $\Phi_\theta^{\text{op}} : (f, g, \Omega) \mapsto \hat{u}^{\text{op}}$, as in neural operator and physics-informed neural operator methods [? 25]. Conditional on a PDE instance P , the prediction is deterministic at inference time, so

$$\text{Var}(\Phi_\theta^{\text{op}}(P)(x) | P) = 0. \quad (8)$$

However, the estimator generally has approximation bias

$$b_\theta(P, x) = \Phi_\theta^{\text{op}}(P)(x) - u(x), \quad (9)$$

so its conditional MSE is

$$\mathbb{E}[(\Phi_\theta^{\text{op}}(P)(x) - u(x))^2 | P] = b_\theta(P, x)^2. \quad (10)$$

Unlike Monte Carlo error, this bias does not decrease with additional inference-time sampling compute. Moreover, under distribution shift, learned PDE solvers can incur substantially larger approximation error because their predictions are tied to the training distribution rather than to an unbiased inference-time estimator [23, 7].

F.3 MC²: Learned Correction of a Monte Carlo Estimator

MC² takes a finite-budget Monte Carlo estimate and optional auxiliary PDE information as input. Let $X_K = (\hat{u}_K, a)$, where a may include the source term, domain mask, boundary information, or PDE parameters. MC² outputs $\tilde{u}_K = \Phi_\theta(X_K)$. The population-optimal corrector under squared loss is the conditional expectation, also known as the regression function or Bayes estimator under squared loss [13]:

$$\Phi^*(X_K)(x) = \mathbb{E}[u(x) \mid X_K]. \quad (11)$$

Equivalently,

$$\Phi^* = \arg \min_{\Phi} \mathbb{E} [\|\Phi(X_K) - u\|_2^2]. \quad (12)$$

This immediately gives a useful comparison to raw WoS. Since the identity map $\Phi(X_K) = \hat{u}_K$ is an admissible candidate in the minimization above, the Bayes-optimal corrector is never worse than raw WoS in population MSE:

$$\mathbb{E} [\|\Phi^*(X_K) - u\|_2^2] \leq \mathbb{E} [\|\hat{u}_K - u\|_2^2]. \quad (13)$$

If X_K also contains every input that a standalone neural operator would use, such that $\Phi_\theta^{\text{op}}(P)$ can be expressed as a measurable function of X_K , then the operator is also an admissible candidate in the minimization, and

$$\mathbb{E} [\|\Phi^*(X_K) - u\|_2^2] \leq \mathbb{E} [\|\Phi_\theta^{\text{op}}(P) - u\|_2^2]. \quad (14)$$

Thus, the optimal corrector dominates both raw Monte Carlo and standalone neural prediction whenever the same information is available. In practice, MC² learns an approximation $\Phi_\theta \approx \Phi^*$, so the guarantee holds up to approximation, optimization, and finite-data error:

$$\mathbb{E} [\|\Phi_\theta(X_K) - u\|_2^2] = \mathbb{E} [\|\Phi^*(X_K) - u\|_2^2] + \mathcal{E}_{\text{approx}}(\theta), \quad (15)$$

where $\mathcal{E}_{\text{approx}}(\theta) \geq 0$ captures the gap between the learned corrector and the Bayes-optimal corrector.

F.4 Variance Reduction from a Lipschitz Corrector

The preceding argument explains why an optimal corrector can reduce MSE. We now show explicitly how a learned corrector reduces Monte Carlo variance.

Assume that Φ_θ is L_θ -Lipschitz in its first argument (holding a fixed) on the support of low-budget Monte Carlo inputs:

$$\|\Phi_\theta(z, a) - \Phi_\theta(z', a)\|_2 \leq L_\theta \|z - z'\|_2. \quad (16)$$

Let \hat{u}'_K be an independent copy of \hat{u}_K conditioned on the same PDE instance P (with the same auxiliary information a). Using the standard identity

$$\text{Var}(Z) = \frac{1}{2} \mathbb{E} [\|Z - Z'\|_2^2] \quad (17)$$

for an independent copy Z' , where Var denotes total variance for vector-valued Z [22], we obtain

$$\text{Var}(\tilde{u}_K \mid P) = \frac{1}{2} \mathbb{E} \left[\|\Phi_\theta(\hat{u}_K, a) - \Phi_\theta(\hat{u}'_K, a)\|_2^2 \mid P \right] \quad (18)$$

$$\leq \frac{L_\theta^2}{2} \mathbb{E} \left[\|\hat{u}_K - \hat{u}'_K\|_2^2 \mid P \right] \quad (19)$$

$$= L_\theta^2 \text{Var}(\hat{u}_K \mid P), \quad (20)$$

where the first equality applies the variance identity to \tilde{u}_K , the inequality applies the Lipschitz bound, and the final equality applies the variance identity to \hat{u}_K . Therefore, if the corrector is contractive on the Monte Carlo noise directions ($L_\theta < 1$ locally on the relevant input distribution), MC² strictly reduces conditional variance:

$$\text{Var}(\tilde{u}_K \mid P) < \text{Var}(\hat{u}_K \mid P). \quad (21)$$

The cost is that the corrected estimator is no longer guaranteed to be unbiased. The pointwise bias is

$$\text{Bias}(\tilde{u}_K(x) \mid P) = \mathbb{E}[\Phi_\theta(\hat{u}_K, a)(x) \mid P] - u(x) \quad (22)$$

and MC² improves over raw WoS in MSE whenever the variance reduction more than compensates for the introduced squared bias:

$$\text{Bias}^2(\tilde{u}_K \mid P) + \text{Var}(\tilde{u}_K \mid P) < \text{Var}(\hat{u}_K \mid P). \quad (23)$$

E.5 Comparison and Asymptotic Behavior

The three estimators occupy different regions of the bias–variance plane. Pure WoS is approximately unbiased and broadly applicable, but its variance decays only as $\mathcal{O}(1/K)$, making high accuracy expensive. Pure neural operators eliminate Monte Carlo variance at inference time but introduce approximation bias that does not vanish with additional sampling compute and may grow under distribution shift [23, 7]. MC^2 starts from an approximately unbiased Monte Carlo estimator and applies a learned correction that reduces finite-sample variance in exchange for controlled bias.

Asymptotic consistency. As $K \rightarrow \infty$, the raw WoS estimator converges to the true solution up to the ε -shell bias. By continuity of Φ_θ ,

$$\tilde{u}_K = \Phi_\theta(\hat{u}_K, a) \rightarrow \Phi_\theta(u, a), \tag{24}$$

so asymptotic consistency requires the corrector to approach the identity on clean inputs: $\Phi_\theta(u, a) \approx u$. Training on multiple Monte Carlo budgets, including high-quality estimates, encourages this behavior heuristically by exposing the corrector to a range of noise levels. We do not prove asymptotic consistency formally; rather, our empirical results demonstrate that in the practical finite-compute regime, the variance reduction from MC^2 substantially outweighs the introduced bias.